Acceleration of Plasma by a Propagating Current Sheet

RODNEY L. BURTON
Department of the Aerospace and Mechanical Engineering Sciences, University of California, San Diego, La Jolla, California
AND
ROBERT G. JAHN
Department of the Aerospace and Mechanical Sciences, Princeton University, Princeton, New Jersey
(Received 7 August 1967; final manuscript received 9 February 1968)

The structure of a propagating current sheet in a linear pinch discharge in argon is examined with magnetic and electric probes, and interpreted from a magnetogasdynamic point of view. From an integration of the $j_z B_\theta$ distributions it is deduced that the bulk of the initial mass fill of the chamber is radially accelerated to the current sheet velocity. Acceleration of ions in the sheet is partially accomplished by a radial electric field, which imparts about half of the necessary energy. The remaining energy is acquired through a $j_z{}^+B_\theta$ force applied to the ions, which are deflected axially as they pass through the sheet, and, therefore, conduct a large fraction of the axial current.

I. INTRODUCTION

Pulsed plasma accelerators, wherein $\mathbf{j} \times \mathbf{B}$ body forces are applied to a gas through the interaction of large discharge currents with their self-induced magnetic fields, have been extensively studied as injectors for thermonuclear machines,[1] and more recently as high performance space thrusters.[2] Although several geometries have been employed, e.g., parallel plate[3] and coaxial accelerators,[4] inverse[5] and linear pinches,[6] the sequence of electromagnetic interactions is the same in each. Namely, capacitively stored energy is abruptly switched across a pair of electrodes separated by ambient gas in the pressure range of 0.01–10 Torr. The gas breaks down, current rises rapidly in the circuit, and the discharge forms as a thin sheet of current, positioned in the chamber to present a minimum inductance configuration to the external circuit. The self-magnetic field enclosed by the circuit then interacts with the discharge current to accelerate the sheet through the ambient gas, ionizing it, and in the proper circumstances, accelerating it to the sheet velocity.

The details of the gas acceleration process and of the current conduction mechanism in the plasma sheet are not yet completely understood. Several models have been proposed to correlate empirical data at various levels of sophistication. The simplest models assume a thin, absorbing or reflecting current sheet (snowplow models),[7] or a sheet-driven shock wave (hydrodynamic or gasdynamic models),[8] and serve primarily to predict the position-time trajectory of the current sheet. More detailed models recognize that the current sheet has a finite thickness with an interior structure. The plasma in the sheet may then be treated as a continuum fluid, characterized by a spatially varying conductivity, density, etc., to which a generalized Ohm's law and momentum equation may be applied. Alternately, the plasma in the sheet may be examined as a collection of particles, whose trajectories are controlled by the prevailing electromagnetic fields and collision events. The latter two approaches have been applied to a theta pinch by Lovberg,[9] whose results clearly display the importance of knowing the electric field, magnetic field, particle density, and temperature profiles in the plasma, before attempting to apply detailed particle models.

This paper describes a series of experiments performed on a large-radius linear pinch discharge in argon, to determine the profiles of interior electric and magnetic fields associated with the propagating current sheet, from which a self-consistent interpretation of the current-conduction and gas-acceleration process might be formulated. The linear pinch configuration is selected for its inherent geometric simplicity, highly reproducible characteristics, and accessibility to detailed diagnostic probing, rather than for any direct technological application. The use of a heavy gas, however, is motivated by an ultimate electric propulsion interest.

[1] J. Marshall, Phys. Fluids **3**, 134 (1960).
[2] S. Domitz, H. G. Kosmahl, P. Ramins, and N. J. Stevens, NASA Technical Note D3332 (1966).
[3] R. H. Lovberg, in *Proceedings of the Sixth International Conference on Ionization Phenomena in Gases*, T. Hubert and E. Crémien, Eds. (Bureau des Editions, Centre d'Etudes Nucléaires de Saclay, Paris, 1964), Vol. IV, p. 235.
[4] R. H. Lovberg, Phys. Fluids **7**, S57 (1964).
[5] G. C. Vlases, J. Fluid Mech. **16**, 82 (1963).
[6] R. G. Jahn and W. von Jaskowsky, AIAA J. 2, 1749 (1964).
[7] R. L. Garwin and M. Rosenbluth, Los Alamos Laboratory Report LA-1850, (1954).
[8] I. Granet and W. J. Guman, Republic Aviation, PPL Report No. 120, (1959).
[9] R. H. Lovberg, AIAA J. 4, 1215 (1966).

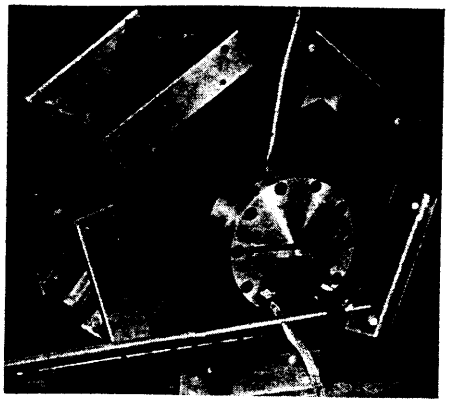

FIG. 1. Linear pinch chamber and capacitor bank. Rotating mirror (streak) photographs are taken through the slit in the anode.

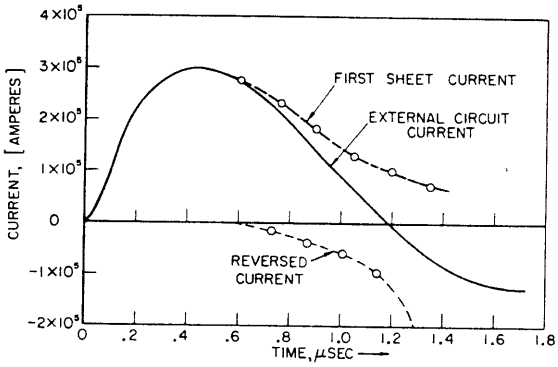

FIG. 2. Current in the discharge circuit versus time. After $t = 0.60$ μsec reverse current flows near the insulator, and external circuit current is less than current in the first sheet.

II. LINEAR PINCH EXPERIMENTS

The 5-in. diam × 2-in. high chamber of the linear pinch device shown in Fig. 1, and described in detail elsewhere,[6] is initially filled with argon test gas at a pressure of 0.12 Torr. A 785-J capacitor bank is charged to 10 kV, and switched across the cylindrical test chamber through a low-inductance gas-triggered discharge switch.[10] The external circuit current is monitored with a Rogowski loop, and is found to approximate a sinusoid of period 2.4 μsec damped by 0.0055 Ω, with an amplitude of 300 000 A on the first half-cycle (Fig. 2). The current sheet arises near the outer insulating wall and is accelerated radially inward toward the chamber axis by the $j_z B_\theta$ interaction in the classical dynamical pinch mode. This inward motion is readily displayed by a sequence of Kerr-cell photographs taken with the radial-view arrangement shown in Fig. 3. The appearance of the discharge at five

[10] R. G. Jahn, W. von Jaskowsky, and A. L. Casini, Rev. Sci. Instr. 36, 101 (1965).

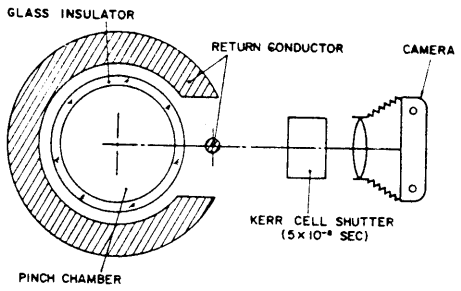

FIG. 3. Arrangement of Kerr-cell shutter and horseshoe conductor for radial-view photographs of the pinch chamber.

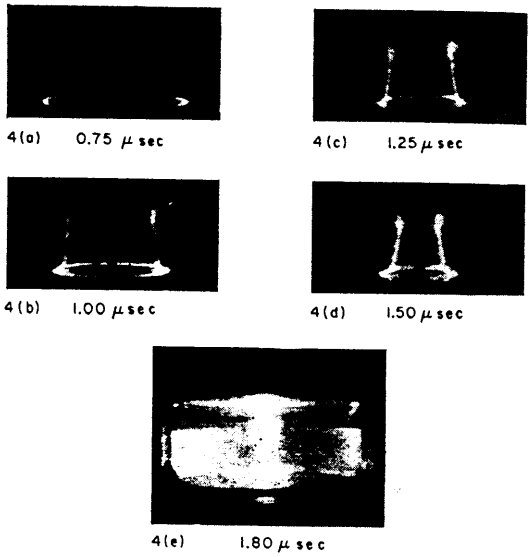

FIG. 4. Radial Kerr-cell photographs of discharge in argon, 0.12 Torr, 10 kV. The top electrode is the anode. The conducting bolt visible in (a), (b), (c), (d), has been removed in (e).

selected times is shown in Fig. 4, wherein the luminosity is seen concentrated in a thin cylindrical shell, uniform over most of the gap and tilted at an angle φ of 0.05–0.10 rad with respect to the chamber axis. Examination of many such photographs, and of complementary axial-view streak photographs, indicates that the luminous front accelerates during the time of current rise ($t < 0.45$ μsec), and subsequently maintains a constant radial propagation velocity U_r of 4.3×10^4 m/sec, a speed which corresponds to an argon atom kinetic energy of 430 eV. To the extent that the luminous front coincides with the current sheet, this constant velocity can simplify the analytical formulation.

To locate the current sheet relative to the luminosity pattern, a small magnetic probe of standard design is inserted axially into the discharge, and the B_θ signal is correlated with the electrical pulse which opens the Kerr cell. Figure 5 displays a

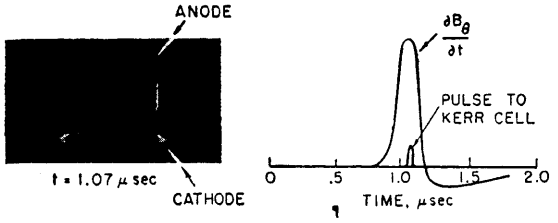

FIG. 5. Luminous front passing over a Pyrex-encased magnetic probe coil, positioned on the midplane. $\partial B_\theta/\partial t$ is a maximum at the time of the photograph.

photograph of the luminous front passing over the Pyrex-encased probe, and the corresponding electrical signals from the probe and Kerr-cell trigger. It is seen that the point of maximum $\partial B/\partial t$, which closely corresponds to the point of maximum current density **j**, is coincident with the thin luminous region. A complete point by point survey of the discharge chamber, taken over a $\frac{1}{8}$-in. increment mesh with a magnetic probe coil of 2-mm diameter, confirms the coincidence of the current density patterns with the luminous patterns over the entire discharge history. Thus it seems reasonable to presume that, in general, the luminosity patterns indicate regions of plasma resistively excited by the discharge current.

Profiles of axial current j_z versus radius and axial position are computed to $\pm 15\%$ accuracy from an extensive sequence of five overlay probe traces.[11] Samples of these profiles are displayed in Fig. 6. On the midplane of the chamber, the current sheet is observed to be less than 1 cm thick and to propagate inward coincidently with the luminous front. Behind the current sheet is a region of low amplitude j_z, flowing in the same direction as current in the sheet. The current density pattern broadens along the anode, and tends to lead the central portion of the sheet slightly. Along the cathode, the current density trails the main sheet slightly, agreeing with the luminous patterns. Because the current density patterns measured on the midplane are nearly independent of sheet position, it is possible to assign a propagation velocity to the magnetic field distribution. Also, current in the sheet decreases for $t > 0.45$ μsec so that the maximum B_θ does not change with radius. The current density and magnetic field are thus constant in time for an observer moving inward at velocity U_s.

The patterns of radial current j_r are determined from the magnetic probe data to $\pm 15\%$ accuracy. Large radial current density, comparable to maximum j_z, is found to be restricted to the cathode

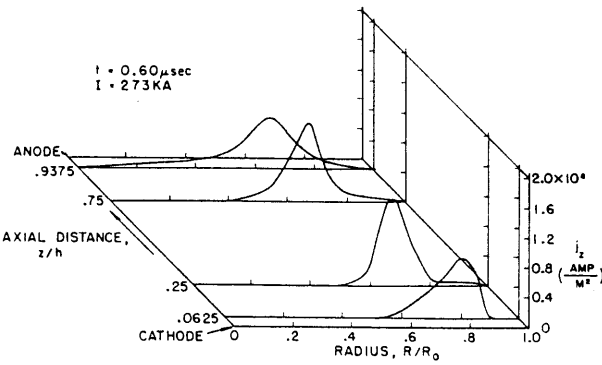

FIG. 6. Distribution of axial current density in the pinch chamber at $t = 0.60$ μ sec.

sheath region. In the central portion of the sheet away from the electrodes, the radial current density is approximately one-tenth of the corresponding axial current density. This is consistent with the observed tilt angle of the luminous front of 0.05–0.10 rad.

The magnitude and direction of the electric field embodied in the current sheet is also determined by a point by point survey over a $\frac{1}{8}$-in. mesh,[11] using a coaxial floating double probe first developed by Burkhardt and Lovberg.[12] This probe measures the difference in plasma potential over a 2-mm electrode separation, from which the electric field distribution may be calculated to within $\pm 10\%$. The axial electric field throughout the discharge displays a pattern which may be closely identified with that of the motional field $U_s B_\theta$, with a maximum amplitude of 450 V/cm. This point is verified by magnetic flux calculations based on the convecting magnetic field distribution, and is further corroborated by an inner voltage divider which measures the voltage drop across the electrodes without enclosing any magnetic flux (Fig. 7). Before the sheet reaches the divider, this drop is on the order of 50 V, which assigns a small fraction of the total circuit resistance, less than 0.00025 Ω, to the discharge, and implies a negligible electrostatic field between the electrodes. Since the magnetic field was found to be constant for an observer moving inward at velocity U_s, it is concluded that the axial electric field as measured in this moving frame is nearly zero.

The electric field seen by an observer moving inward at velocity U_s is, therefore, almost purely radial. Measurements show that the E_r field patterns convect radially inward with the patterns of $j_z B_\theta$ and attain a maximum amplitude in the sheet of several hundred volts/centimeter (Fig. 8). The

[11] R. L. Burton, Ph. D. Thesis, Princeton University (1966).

[12] L. C. Burkhardt and R. H. Lovberg, Phys. Fluids 5, 341 (1962).

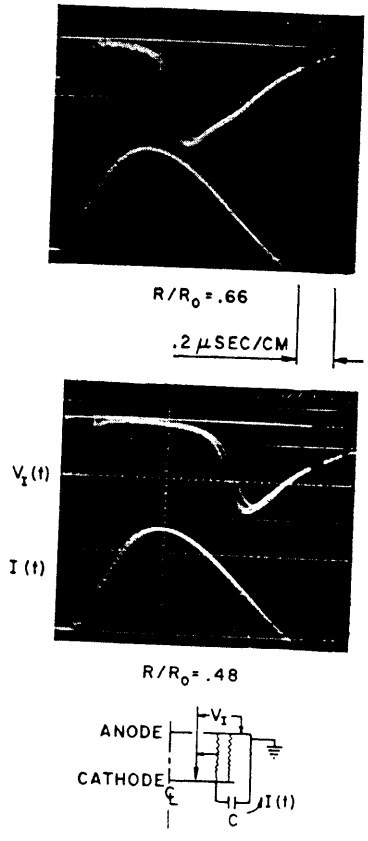

FIG. 7. Voltage signal of the inner divider at 2 radii. The resistive component measured at early times is about 50 V. Maximum voltage is 2300 V.

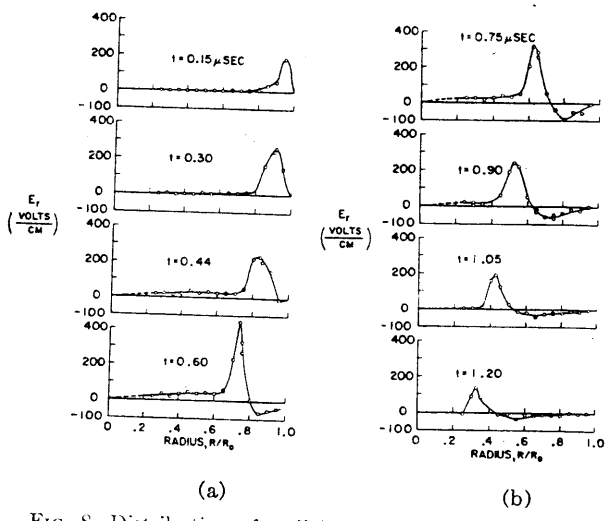

FIG. 8. Distribution of radial electric field versus radius, from 0.15–1.20 μsec. The peaked portion of the distribution corresponds to E_r pointing radially inward.

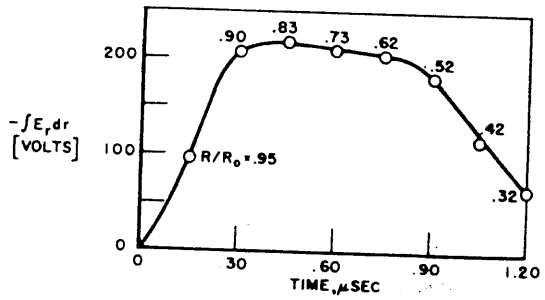

FIG. 9. Voltage drop across the current sheet $\int E_r\, dr$, as a function of time. An argon ion streaming into the sheet (at 430 eV) acquires this amount of electrostatic potential. The curve is labeled showing the radial position of the current sheet at the time the voltage was measured.

electric field profiles also show that the sign of E_r reverses in the wake of the sheet. The direction of the field is such that ions entering the sheet are first accelerated radially inward, and then radially outward. Finally, simultaneous electric and magnetic probe measurements at all radii show that the maxima of the laboratory-measured E_r, E_z, and $j_z B_\theta$ distributions occur at the same time for a given radial position.

In the absence of an explicit electron density measurement, the ionization process at the front of the sheet can only be hypothesized. On the basis of spatially resolved spectroscopic measurements, which show doubly ionized argon at all radii, and from estimates of the local resistive heating, the electron temperature is probably 3 to 5 eV, a value which allows ionization of incoming particles near the sheet leading edge by inelastic electron–atom collisions. If this ionization indeed occurs near the leading edge of the sheet, the total voltage difference radially through the sheet represents the potential energy gained by each ion traversing the sheet, and can be compared with the energy of a particle streaming into the sheet (430 eV) by integrating the distributions of E_r versus radius. Figure 9 displays a plot of this voltage difference obtained by integration across the sharply peaked portion of the distribution, where E_r points inward. The ion electrostatic potential gain is never more than 200 V, less than half of the ion streaming energy. If the ion is initially created in the middle of the sheet, or is allowed to move into the wake region of reversed field behind the sheet, its electrostatic potential energy decreases below 200 V, and it clearly becomes impossible for the ion to achieve sheet velocity by electrostatic acceleration in the radial electric field.

This disparity between sheet accelerating potential and particle streaming energy is in agreement with the measurements of the $j_z B_\theta$ force density in the region behind the sheet. Upon integration of $j_z B_\theta$ over this volume, i.e., between the radius of maxi-

mum B_θ field and the chamber wall, a substantial radial accelerating force is found, equal to one-third of the integral of $j_z B_\theta$ for the entire chamber. The measurements of $j_z B_\theta$, therefore, are consistent with those of E_r, since both measurements imply that ions are only partially accelerated in the sheet.

The $j_z B_\theta$ measurements also imply, however, that nearly all particles originally in the chamber achieve the sheet velocity U_s. After integration of $j_z B_\theta$ over the chamber volume to give the radial force F_r, a subsequent time integration of F_r yields the total electromagnetic impulse I_m applied to the gas up to the time of pinch. The coupling between the driving current and the mass of test gas m_0 can then be defined by a "sweeping efficiency," $I_m/m_0 U_s$. The sweeping efficiency for the discharge is found to be 96%, implying that very little mass escapes complete entrainment. Since the electric field E_r provides only partial acceleration, an additional mechanism must be responsible for bringing the ions to the sheet velocity.

III. SUMMARY OF THE CURRENT SHEET STRUCTURE

Referring to Fig. 10, the experimental evidence suggests that a variety of processes take place in the current sheet. For an observer moving with the sheet, cold argon atoms enter the sheet and are rapidly ionized. The resulting ions and electrons then encounter a region of radial electric field and azimuthal magnetic field. The Hall parameter of the electrons is calculated to be larger than unity everywhere except at the very front of the sheet, and, once substantial ionization is achieved, the ion Hall parameter is effectively infinite, because ion-neutral collisions are rare. Both ions and electrons can, therefore, be expected to conduct current.

The Larmor radius of the electrons is sufficiently small (10^{-3} cm), so that the electrons gyrate in a nearly constant $\mathbf{E} \times \mathbf{B}$ field. However, the Larmor radius of the ions at the center of the sheet is 4 cm, and at the back of the sheet is 1 cm or less. The trajectory of the ions through the regions of B_θ gradient and fluctuating E_r field is thus quite complex. Since the pinch time is on the order of the reciprocal ion gyrofrequency, most of the ions do not have time to execute a full gyration.

The gasdynamic pressure gradient in the sheet further complicates this picture (Fig. 10). The pressure is nearly zero at the sheet leading edge, rises rapidly in the sheet as the ions are decelerated, and then decreases to a low value at the outside wall. The maximum pressure exerted by the ions may be

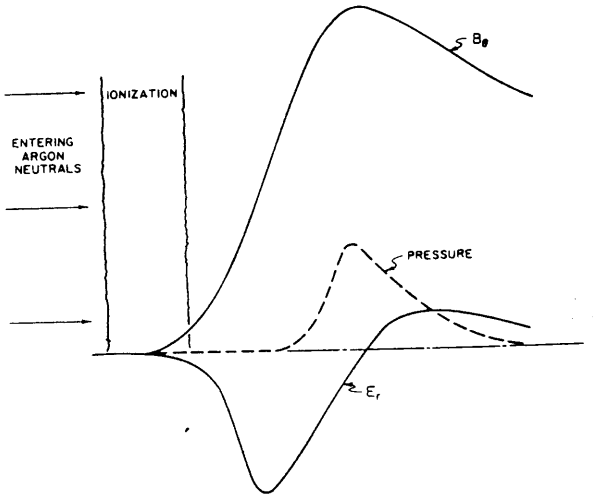

FIG. 10. Structure in the frame of the current sheet. The argon is presumed to be highly ionized at the leading edge. Sheet width is small compared to sheet radial position. The pressure profile is estimated, as discussed in the text.

estimated by a simple one-dimensional steady model, applied to the frame moving with the sheet. For sheet positions greater than 2 cm, where radius effects can be neglected, the radial momentum equation is integrated directly from the sheet leading edge (1) to the point of maximum pressure (2). Assuming that p_1 and B_1 are approximately zero,

$$p_2 \approx n_1 M_+ U_1^2 - n_2 M_+ U_2^2 - \frac{B_2^2}{2\mu_0}, \qquad (1)$$

where n is the charged-particle density. Assuming that complete ionization of incoming particles occurs at (1), and that these particles enter at velocity U_s and ambient density n_A, the one-dimensional steady-flow continuity equation is written

$$n_1 U_1 = n_A U_s = n_2 U_2, \qquad (2)$$

so that

$$p_2 \approx n_A M_+ U_s^2 \left(1 - \frac{n_A}{n_2}\right) - \frac{B_2^2}{2\mu_0}. \qquad (3)$$

Inserting reasonable values of n_A, U_s, and B_2 into Eq. (3), the pressure p_2 is found to be on the order of the magnetic pressure for a compression on the order of $n_2/n_A = 4$. A density rise of a factor of 4 is the lowest that could be expected for this model; the rise may in fact be larger, depending on the effective specific heat of the plasma. This density rise thus predicates a pressure rise of a factor of 10^4 across the sheet, due mostly to the large temperature increase of the ions, and partially to the density increase. By the assumptions of the present

model, the ion enthalpy becomes

$$h_2 \approx \tfrac{1}{2}U_z^2\left[1 - \left(\frac{n_A}{n_2}\right)^2\right], \tag{4}$$

so that a rise in density by a factor of 4 will convert essentially all of the streaming energy to enthalpy. Depending on the effective plasma specific heat, the temperature of the ions will be 5–50 times larger than that of the electrons. The assumption that the ion swarm has a temperature is valid, because the mean free path for ion–ion collisions is an order of magnitude smaller than the Larmor radius and the current sheet width.

Whatever the maximum pressure level achieved by the ions, it is clear from Fig. 10 that the pressure gradient can have no net accelerating effect on the ion bulk, because of the near-zero-pressure boundary conditions on the chamber wall and axis. The major effect of the pressure gradient, assisted by the E_r field, is to raise the ion enthalpy and reduce the radial streaming velocity in a narrow region at the rear of the current sheet. Given enough time, the ions will eventually pass through the high enthalpy region, but its existence is important in an electric propulsion application, because it is a potential source of frozen flow loss in a thruster.

A consistent interpretation of the E_r and B_θ measurements can be made by first writing the z component of the momentum equation for the plasma in the frame moving with the current sheet

$$nM_+U_r\frac{dU_z}{dr} = j_rB_\theta, \tag{5}$$

where the axial velocity U_z is zero at the sheet leading edge, electron mass is neglected, the flow is assumed steady in the moving sheet frame, and the axial pressure and velocity gradients are assumed negligible. Equation (5) states that if $j_r = 0$ the ions will not acquire any axial velocity U_z, and, therefore, will not conduct current. However, if the radial current is nonzero, as is the case in this experiment, the current sheet is by definition tilted with respect to the chamber axis, and Eq. (5), therefore, implies that tilting of the current sheet is evidence of axial ion velocity and current.

It is instructive to consider Ohm's law in the reference frame moving with the current sheet. In the one-dimensional limit of large radius of curvature, and neglecting the gradient of electron pressure, Ohm's law is written

$$\mathbf{j} = \sigma\cdot[\mathbf{E} + \mathbf{U} \times \mathbf{B}], \tag{6}$$

where $\mathbf{E}$, $\mathbf{B}$, and $\mathbf{j}$ are measured in the moving sheet frame, and $\mathbf{U}$ is the plasma center-of-mass (ion) velocity in this frame. The electron conductivity tensor may be written in the usual form if applied to a right-handed (r, z, θ) coordinate system, with the magnetic field parallel to the θ axis

$$\sigma = \begin{bmatrix} \sigma_{rr} & \sigma_{rz} & 0 \\ \sigma_{zr} & \sigma_{zz} & 0 \\ 0 & 0 & \sigma_{\theta\theta} \end{bmatrix} = \frac{\sigma_0}{1+\Omega^2}\begin{bmatrix} 1 & -\Omega & 0 \\ \Omega & 1 & 0 \\ 0 & 0 & 1+\Omega^2 \end{bmatrix}, \tag{7}$$

where $\sigma_0 = ne^2/m_e\nu_c$, $\Omega = eB/m_e\nu_c$, and ν_c is the electron–ion elastic collision frequency. This gives a current density

$$\mathbf{j} = \frac{\sigma_0}{1+\Omega^2}[E_r + \Omega(U_rB_\theta - E_z) + U_zB_\theta]\hat{r} + \frac{\sigma_0}{1+\Omega^2}[\Omega E_r - (U_rB_\theta - E_z) + \Omega U_zB_\theta]\hat{z}. \tag{8}$$

Equation (8) is now applied to an orthogonal current sheet. If $j_r = 0$ (which as discussed above requires $U_z = 0$), then Eq. (8) yields an axial current j_z (conducted solely by electrons) of

$$j_z = j_z^- = \frac{\sigma_0 E_r}{\Omega} = en\frac{E_r}{B_\theta}. \tag{9}$$

Equation (9) can be used to evaluate the electron density in the current sheet, to the approximation that the ion axial velocity and current sheet tilt are zero. These conditions are nearly met at the peak of the E_r distribution, and experimental measurements of j_z, maximum E_r, and B_θ give an electron density $n = 3 \pm 1 \times 10^{16}$ cm^{-3}, which is 5–10 times the ambient density n_A at 0.12 Torr. This large electron density jump is further evidence that the argon is nearly fully ionized in the sheet, and also indicates that a large pressure gradient is present in the sheet, as discussed above.

Although electrons conduct most of the current in the peaked portion of the sheet, it is clear from Eq. (9) that they cannot do so behind the sheet because of the observed reversal in direction of the E_r field (Fig. 8), which also reverses the electron current. Since the j_z measurements show that the net current does not reverse in and behind the sheet, it must be concluded that the magnitude of the axial ion current density exceeds that of the reversed electron current in the sheet wake. This confirms the above argument that the axial flow velocity U_z

is not zero, as a consequence of the tilted current sheet, and ions are expected to accumulate along the cathode, as has been observed by other experimenters. The magnitude of U_z can be estimated by integrating the z-momentum equation [Eq. (5)] through the sheet, assuming $nU_r = \text{const}$ and $j_r = \varphi j_z$. The result is that $U_z \approx \varphi U_r$, implying that the axial (and radial) streaming energy of the ions is small in the wake region. The ion energy must, therefore, be split nearly equally between electrostatic potential and thermal energy.

IV. SUMMARY

It appears that two separate mechanisms contribute to the radial ion acceleration. In the peaked portion of the sheet the ions flow nearly radially and the axial current is conducted mainly by electrons, while the ions acquire electrostatic energy from the E_r field. This increase in ion energy is accompanied by a nearly equal increase in enthalpy, and by an ever-increasing axial deflection determined by $j_r B_\theta$. Behind the sheet a $j_z^+ B_\theta$ force is applied directly to the ions as they conduct axial current toward the cathode, and they are thus accelerated to full sheet velocity. As pointed out in a separate calculation,[13] the ion enthalpy increase introduces a loss of dynamic efficiency into the acceleration process, a loss which can be decreased by designing the current sheet to accelerate strongly into a nonuniform ambient density distribution. Extension of the experiments into such a domain is clearly indicated.

ACKNOWLEDGMENTS

The authors wish to thank W. von Jaskowsky and A. L. Casini for their help in performing the experiments and interpreting the results. They also gratefully acknowledge many fruitful discussions with R. H. Lovberg.

This work was performed at Princeton University under the support of National Aeronautics and Space Administration Grant NsG-306063, and at the University of California, San Diego, under the support of the Institute for Pure and Applied Physical Sciences.

[13] N. A. Black and R. G. Jahn, AIAA J. 3, 1209 (1965).